Research Article

Wang Hailun* and Alexander Martinez

Application of modified culture Kalman filter in bearing fault diagnosis

https://doi.org/10.1515/phys-2018-0095
Received Jul 29, 2018; accepted Aug 19, 2018

Abstract: Rolling bearings are an important part of rotary machines. They are used most widely in various mechanical sectors, which are among the most vulnerable components in machines. This paper uses CKF algorithm to compile a signal analysis system, analyses the vibration signal of the rolling bearing, extracts fault features, and realizes fault diagnosis. In order to improve the estimation accuracy of bearing fault diagnosis under nonlinear model, a nonlinear model of bearing fault diagnosis based on quaternion and low-accuracy high-noise sensors is established, and the attitude estimation has performed using the culture Kalman filter (CKF) algorithm. The sensor data comparison shows that the use of the volumetric Kalman filter algorithm can effectively improve the estimation accuracy of bearing fault diagnosis and stability. In this paper, the measured vibration signals of several groups of rolling bearings are analysed, and the signal characteristic frequency has extracted. The results show that using the analysis software designed in this paper, several typical faults of rolling bearings can be correctly identified.

Keywords: Rolling bearing, fault diagnosis, vibration signal, CKF

PACS: 02.30.Cj, 02.30.Sa, 07.10.-h

1 Introduction

With the development of science and technology, modern industry is gradually making large-scale, complex, high-speed, and automated production equipment. It has great advantages in increasing productivity, lowering costs, saving energy, reducing scrap rate, and ensuring product quality [1]. However, catastrophic accidents caused by failures and the resulting loss of life and property and damage to the environment are also serious [2], which has led to people's influence on such things as aerospace vehicles, nuclear power plants, thermal power plants and others. The reliability and safety of large-scale chemical equipment have raised higher requirements. In addition to improving the system reliability and safety of reliability design, researching and applying new materials, new processes, and strengthening quality control measures in the production process during the design and manufacturing stages, the system reliability and safety are improved. An important approach is to monitor and diagnose the working status of the system in real time, which helps to achieve effective control of the equipment and provide early warning of the occurrence of catastrophic failures, and provide effective information for taking corresponding remedial measures [3]. Fault diagnosis theory has developed to meet the requirements of system reliability and safety requirements, and to reduce and control the occurrence of catastrophic accidents [4]. Therefore, the development of fault diagnosis theory will inevitably promote the rapid development and widespread application of fault monitoring and monitoring systems, which can further improve the reliability and safety of system operation, and thus produce huge economic and social benefits [5, 6].

Compared with other mechanical components, rolling bearings have a unique feature, that is, its life is discrete [7]. Due to this feature of the bearing, there will be such a situation: some bearings have already exceeded their design life and can still work normally, and some bearings fail to reach their design life and appear various failures. Therefore, if the bearing is regularly repaired according to its design life, on the one hand, the bearing that exceeds the design life but still works will be removed for disposal, resulting in waste; on the other hand, bearings that fail to reach the design life will fail. The timely discovery has not removed until regular maintenance and was scrapped. This made the machine work less accurately after a bearing failure and before it was scrapped, or a serious failure occurred without maintenance time, resulting

***Corresponding Author: Wang Hailun:** Shanghai Maritime University, Logistics Engineering College, Quzhou University, College of Electrical and Information Engineering, Shanghai 200135, China
Email: wanghl@qzu.zj.cn
Alexander Martinez: Newcastle University, School of Computing, Newcastle upon Tyne NE1 7RU, United Kingdom;
Email: Martinez.Ashoufeng@newcastle.ac.uk

in the entire machine being in a paralysed state[8]. Therefore, the early detection and fault diagnosis of the rolling bearing working status and faults have important practical significance for the safe and stable operation of the equipment [9].

With the ever-increasing speed, automation, large-scale, and complicated modern mechanical equipment, people are increasingly demanding the safety and reliability of mechanical equipment. Once the mechanical equipment is out of order, it will have a huge impact on production and quality. It even poses a threat to people's lives [10]. Bearing fault diagnosis and adjustment is the bottleneck of the improvement of bearing operation efficiency, involving three important links such as alignment, rolling and anti-shake. Bearing fault diagnosis has usually represented by rotation angle, tilt angle and roll angle, which provides operators with spreaders. The attitude information guides the loading and unloading operation of the bearing, and provides the attitude parameter data for the control system to ensure the safety of the loading and unloading process.

In view of this, this study will introduce the CKF pose estimation link into the control system. The basic idea is to use the CKF algorithm to calculate the pose estimation and attitude measurement signals of the previous stage to obtain the optimal pose estimation. The controller performs attitude adjustment control. This method can theoretically achieve two effects. (1) The attitude control signal provided to the controller is the best estimate of the original attitude development trend, with reasonable advance analysis and The pre-judgment property makes the control system have attitude adjustment convergence properties, and the system becomes stable. (2) We can reduce the passive disturbance (mechanical vibration and wind speed influence) outside the control system of the bearing fault diagnosis and the sensor self-noise interference of the measurement-monitoring unit to avoid these disturbances during the repetitive attitude adjustment, thereby affecting the system stability [11]. The bearing fault diagnosis control system is a large inertia flexible load, and the application of the CKF algorithm has not yet been seen in this field. Therefore, this paper uses the CKF algorithm to solve the bearing fault diagnosis based on the quaternion method, using a three-axis gyroscope. The triaxial acceleration sensor acquires sensor data from the bearing fault diagnosis and control test device, and applies the CKF algorithm to the bearing fault diagnosis and diagnosis. To find the comparison object, the SBG AHRS sensor produced by SBG Systems of France is used as the monitoring standard of bearing fault diagnosis.

2 Rolling bearing fault diagnosis and CKF methodology

2.1 Failure mechanism and characteristic frequency of rolling bearings

2.1.1 Analysis of causes of vibration of rolling bearings

Caused by the vibration and noise of rolling bearings, in addition to external excitation factors (such as the rotor is not stable, misalignment, fluid excitation, structural resonance and other vibration transmission), the internal vibration of the bearing can be divided into the following three types [12].

The first type is due to the vibration of the bearing structure itself. This section includes two points.

1. The rolling body vibration through the direction of the load;
2. The natural vibration of the ring;
3. The vibration caused by the elastic characteristics of the bearing.

The second type is caused by bearing shape and accuracy problems. This section includes two things.

1. Vibration caused by waviness of rings, raceways and rolling elements;
2. The rolling body size is uneven, the outer ring eccentric vibration;

The third type of vibration caused by improper use of bearings or improper assembly. This section includes three points.

1. Vibration caused by local defects in the contact surface of the raceway;
2. Poor lubrication, vibration caused by friction;
3. The assembly is not correct, vibration caused by deflection of the journal.

2.1.2 Calculation frequency of rolling bearing faults

When the rolling element meets a local defect at the contact with the raceway, an impact signal is generated. Defects on different components, the contact point through the frequency of the defect is not the same, this frequency is called the impact of the interval frequency and characteristic frequency. The interval frequency can be obtained from the analysis of the simple kinematics of the bearing based on the bearing rotation speed and the size of the bearing parts.

There are contact points A and B on the raceways of the outer ring and inner ring, respectively, as shown in Figure 1. If the radial clearance is zero, the circumferential speeds of point A and point B are respectively.

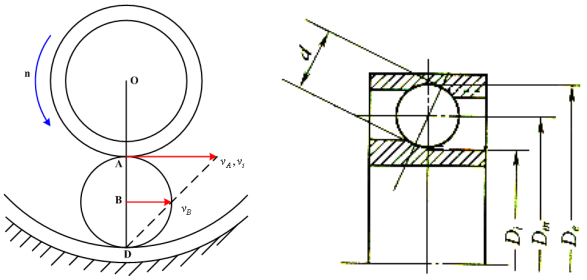

Figure 1: The relationship of the components in the rolling bearing

$$Ve = \left(\frac{\pi_{De}}{60}\right)_{ne} \tag{1}$$

$$Vi = \left(\frac{\pi_{Di}}{60}\right)_{ni} \tag{2}$$

In the formula, V_e , V_i - the circumferential speed at the outer ring and inner ring raceway contact point, mm/s; D_e , D_i - the diameter at the outer ring, inner ring raceway contact point, mm; n_e , n_i - the outer ring, inner ring speed, r /min.

$$\gamma = \left(\frac{d}{D_m}\right) cos\alpha \tag{3}$$

In the formula d - rolling element diameter, mm; D_m - rolling element diameter of centre circle, mm; α - contact angle, reflecting the centreline of the contact point and the centreline of the rolling element in the axial direction of the bearing, rad.

$$D_e = D_m + dcos\alpha = D_m(1+\gamma) \tag{4}$$

The revolution speed of the rolling elements around the bearing centreline is the average of the speeds V_i and V_e .

$$V_e = \frac{V_i + V_e}{2} = \frac{\pi}{120} D_m[n_i(1-\gamma) + n_e(1+\gamma)] \tag{5}$$

The revolution speed of the rolling element is also the linear velocity of the cage centre circle. The line speed at a certain point on the cage centre circle is as follows.

$$V_e = \frac{\pi D_m}{60} n_e \tag{6}$$

From the above, the rotational speed of the cage is as follows.

$$n_e = \frac{1}{2}[n_i(1-\gamma) + n_e(1+\gamma)] \tag{7}$$

The rotation speed of the inner ring relative to the cage is as follows.

$$n_{ie} = n_i - n_e = \frac{1}{2}(n_i - n_e)(1-\gamma) \tag{8}$$

The rotational speeds of the inner and outer rings with respect to the cage are as follows.

$$n_{ec} = n_e - n_c = \frac{1}{2}(n_e - n_c)(1-\gamma) \tag{9}$$

The rotation speed n_o of the rolling element can be obtained from the relationship between the linear velocities of the two objects at the contact point. For example, the linear velocity at the B point where the rolling element encounters the inner ring is as follows.

$$V_{OB} = -\frac{2\pi n_o}{60} \times \frac{d}{2} \tag{10}$$

The negative sign in the formula indicates that the linear velocity of point B with respect to the centre of the rolling element in which the rolling element contacts the rolling element is as follows.

$$V_{iB} = -\frac{2\pi(n_i - n_e)}{60} \times \frac{D_i}{2} \tag{11}$$

According to the pure rolling condition, the corresponding point B speed on the rolling contact point B and the inner ring raceway is equal.

$$V_{iB} = V_{OB} \tag{12}$$

The characteristic frequency of the shock vibration caused by local defects is as follows. Frequency of fault features when the inner ring is defective[13].

$$f_i = \frac{n}{120}(1 + \frac{d}{D_m} cos\alpha)z \tag{13}$$

Fault feature frequency of the outer ring is defective.

$$f_e = \frac{n}{120}\left(1 - \frac{d}{D_m} cos\alpha\right) z \tag{14}$$

Fault feature frequency of the ball is defective.

$$f_0 = \frac{n}{60}\frac{D_m}{d}\left(1 - \frac{d^2}{D_m^2} cos^2\alpha\right) \tag{15}$$

The fault feature frequency of the cage hitting the outer ring.

$$f_{ec} = \frac{n}{120}\left(1 - \frac{d}{D_m} cos\alpha\right) \tag{16}$$

The fault feature frequency of the cage inner ring is as follows.

$$f_{ic} = \frac{n}{120}\left(1 + \frac{d}{D_m} cos\alpha\right) \tag{17}$$

2.2 CKF derivation process

In order to alleviate the problem of filter divergence and numerical precision caused by rounding errors in the filtering process, the square root version of CKF has developed. CKF essentially propagates the square root of the error variance matrix, thus avoiding the matrix square root calculation and ensuring the variance matrix. The following summarizes the CKF algorithm [14]. Since the square root of the variance matrix in the general CKF is the Cholesky decomposition, this requires that the variance matrix is a positive definite symmetric matrix for unique decomposition. The QR decomposition only requires the matrix full rank or row full rank, so the CKF can be guaranteed to proceed.

$S_{k-1|k-1}$ is known and available, you can directly calculate Cubature points (i=1,2,...,m).

$$\chi_{i,k-1|k-1} = S_{k-1|k-1}\xi_i + \$_{k-1|k-1} \tag{18}$$

The point of propagation of Cubature through the equation of state is as follows.

$$\chi^{\star}_{i,k|k-1} = f(\chi_{i,k-1|k-1}) \tag{19}$$

We can estimate the state prediction at time k.

$$\$_{k|k-1} = \frac{1}{m}\sum_{i=1}^{m}\chi^{\star}_{i,k|k-1} \tag{20}$$

The square root of the estimated error covariance matrix is as follows.

$$S_{k-1|k-1} = Tria([\chi^{\star}_{k|k-1}S_{Q,k-1}]) \tag{21}$$

Hence, $Q_{k-1} = S_{Qk-1}S^{T}_{Qk-1}$,

$$\chi^{\star}_{k|k-1} = \frac{1}{\sqrt{m}}[\chi^{\star}_{1,k|k-1} - \$_{k|k-1}\chi^{\star}_{2,k|k-1} - \$_{k|k-1} \cdots \chi^{\star}_{m,k|k-1} - \$_{k|k-1}] \tag{22}$$

We can directly calculate Cubature points (i=1,2,...,m).

$$\chi_{i,k|k-1} = S_{k|k-1}\xi_i + \$_{k|k-1} \tag{23}$$

We can spread the Cubature points by observing the equations.

$$Z^{\star}_{i,k|k-1} = h(\chi_{i,k|k-1}) \tag{24}$$

It is estimating observations at time k.

$$\$_{Z_{k|k-1}} = \frac{1}{m}\sum i = 1^{m} Z^{\star}_{i,k|k-1} \tag{25}$$

It is estimated autocorrelation covariance matrix.

$$S_{ZZ,k|k-1} = Tria([Z_{k|k-1}S_{R,k}]) \tag{26}$$

Hence, $R_k = S_{R,k}S^{T}_{R,k}$,Because of the inverse operation involved, so QR decomposition is as follows.

$$Z_{k|k-1} = \frac{1}{\sqrt{m}}[Z_{1,k|k-1} - \$_{Zk|k-1}Z_{2,k|k-1} - \$_{Zk|k-1} \cdots Z_{m,k|k-1} - \$_{Zk|k-1}] \tag{27}$$

3 Design of vibration signal analysis system based on CKF

3.1 Overall system design

Based on the knowledge of the local mean and the knowledge of rolling bearing fault diagnosis, the structure of the CKF-based fault diagnosis system has designed in this paper. This paper uses MATLAB to write CKF decomposition algorithm. The function of decomposing the vibration signal of the rolling bearing is realized, which helps to obtain the instantaneous amplitude A of the PF component, the residual U, the pure frequency modulation function SI and the PF component with characteristic features [15]. In order to facilitate the user to analyse the vibration signal of the rolling bearing, CKF-based rolling bearing fault diagnose software is designed by the MATLAB GUI tool. Data file selection, parameter design, feature frequency calculation, display of CKF decomposed components, and feature frequency extraction are realized.

3.2 CKF algorithm program implementation

The key to this system is the specific programming of the CKF algorithm. According to the analysis in this paper, the steps for implementing the local mean decomposition method are as follows.

1. Find out the extreme points of the data sequence.
2. Use the moving average method to process each extreme point to obtain the first local mean function m_{11} and envelope estimation function a_{11}.
3. Using the local average function m_{11} helps to separate the original signal to get the residual signal h_{11}.
4. Use the residual signal and envelope estimation function to get si_{11}.
5. Set the offset value to cycle until the termination condition is met, i.e. SI is a pure FM function.
6. After the decomposition, the PF component, the residual quantity U, the envelope function A, and the pure frequency function SI are returned.

The flowchart of the algorithm implemented in this paper is shown in Figure 2.

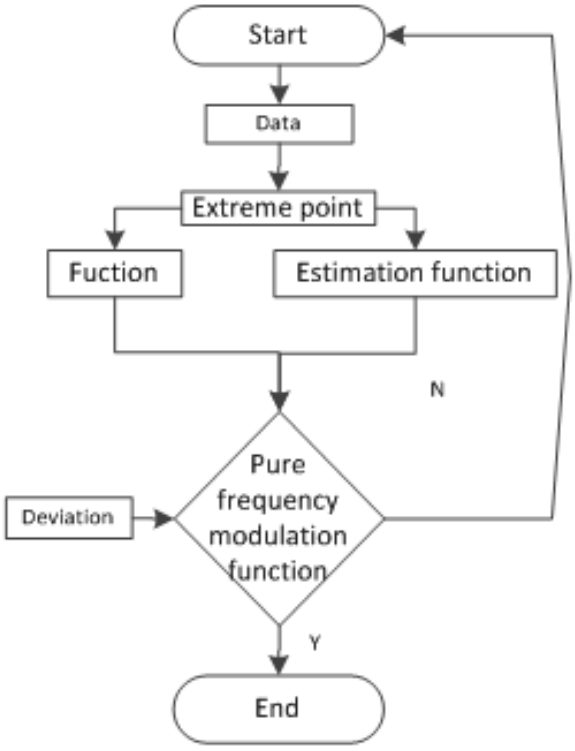

Figure 2: CKF algorithm design flow chart

The designed software is used to analyse the measured rolling bearing vibration signal, and the frequency components of the vibration signal are presented, and compared with the theoretically calculated frequency of the fault characteristic to realize the simple identification of the fault and verify the accuracy and reliability of the software designed in this paper.

3.3 Test data description

The measured data in this paper comes from the Case Western Reserve University Rolling Bearing Fault Data Centre. The test stand consists of a 2-horsepower motor (left), a torque converter/encoder, a dynamometer (right), and control electronics [13–15]. The test bearing supports the motor shaft. A single point of failure was introduced into the failed test bearing using EDM for 7 mil, 14 mil, 21 mil, 28 mil, and 40 mil (1 mil = 0.001 inch) diameters. SKF bearings were used for 7, 14 and 21 mil diameter failures, and NTN equivalent bearings were used for 28 mil and 40 mil failures.

An accelerometer is attached to the vibration data acquisition with the magnetic base housing. The accelerometer is placed at the 12 o'clock position at the two drive ends and the fan end of the motor housing. In some experiments, the accelerometer was mounted on a motor support base plate as well. The 16-channel DAT recorder was used to acquire the vibration signal and post-process it in a MATLAB environment. All data files are in MATLAB (*.mat) format. Digital data was collected at 12,000 samples per second, and data was collected at 48,000 samples per second for faults at the drive end bearing. Use the torque sensor/encoder to collect the speed and horsepower data and record the hand. The failure of the outer raceway is a fixed disadvantage, so that the placement of the fault in the load zone with respect to the bearing has a direct effect on the vibration response of the motor/bearing system. To quantify this effect, experiments were performed with bearings located at 3 o'clock (directly in the load zone), at 6 o'clock (perpendicular to the load zone) and at 12 o'clock on the outer race fault fan and drive end.

3.4 Measure bearing vibration signal and fault diagnosis

3.4.1 Inner ring fault vibration signal analysis

The vibration signal analysed software designed in this paper to analyse the test data to obtain Figure 3. The top of the software shows the time domain and frequency domain waveforms of the inner ring fault vibration signal [16]. The lower part of the software shows the power spectrum of the first four momentary amplitudes of the PF component obtained after the vibration signal is decomposed by CKF, from A1, A2. The characteristic frequency of the inner ring fault can be seen in the A3 power spectrum as 157.5 Hz.

Figure 3 show the PF1 component diagram, Figure 4 shows the A1 component diagram and Figure 5 gives the A1-A4 power spectrum enlargement of the inner ring fault vibration signal.

It can be seen from Figure 5 that the characteristic frequency extracted from the power spectrum obtained by decomposing the signal, the CKF is 157.5 Hz, and the theoretical frequency calculated from the bearing parameters of the test data is 157.9 Hz. Hence, the error rate is 0.25%, we can accurately determine the inner ring fault, which is consistent with the theory [17].

From the vibration signal analysed software of the power spectrum, we can see that A1 power spectrum

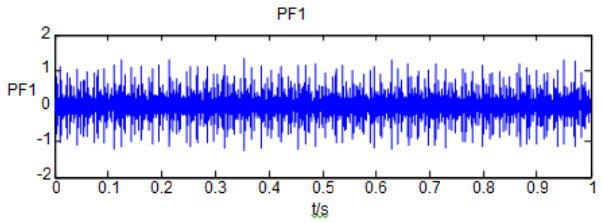

Figure 3: PF1 component of inner ring failure

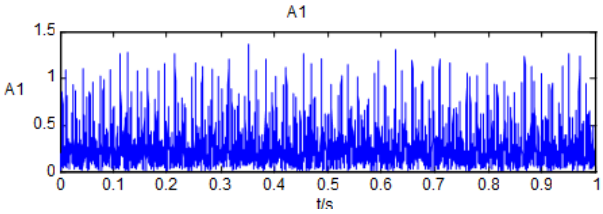

Figure 4: A1 component of inner ring fault

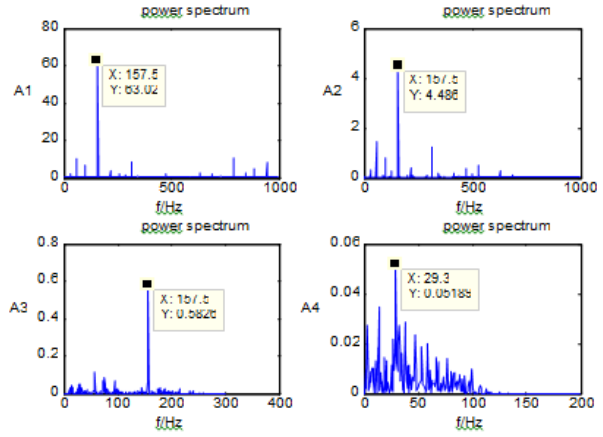

Figure 5: Inner Ring Faults A1, A2, A3, A4 Power Spectrum Enlargement

contains the fault feature frequency accompanied by frequency multiplication, which also contains some frequency; A2 power spectrum also contains the fault feature frequency with frequency multiplication. However, the frequency is more than that of A1. The A3 power spectrum contains the characteristic frequency without frequency multiplication, but the frequency is more; the A4 power spectrum does not include the characteristic frequency. Therefore, by comparison, the power spectrum of the instantaneous amplitude A1 of the PF1 component works best. This may be because the first PF component completely reflects the intrinsic nature of the signal, while the other PF components have separated by the first component.

3.4.2 Vibration signal analysis of outer ring faults

Using the designed vibration signal analysed software to analyse the test data is shown in Figure 4-5. The top of the software shows the time domain and frequency domain waveforms of the outer ring fault vibration signal [18]. The bottom of the software shows the power spectrum of the first four instantaneous amplitudes of the PF component obtained after the vibration signal is decomposed by the CKF. In the A3 power spectrum, the characteristic frequency of the inner ring fault can be seen as 104.7 Hz.. Figure 6, Figure 6, and Figure 8 show the PF1 component diagram, A1 component diagram, and A1 power spectrum diagram of the outer ring fault vibration signal, respectively.

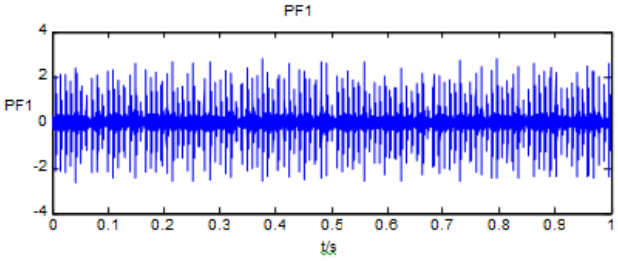

Figure 6: PF1 component diagram of outer ring fault

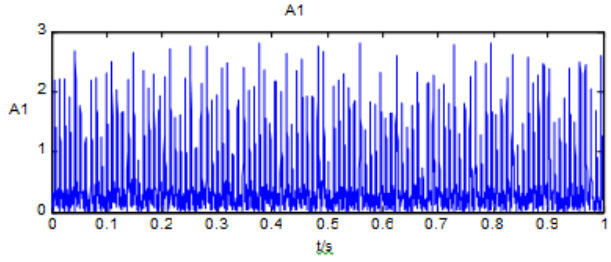

Figure 7: Outer ring fault A1 component diagram

It can be seen from Figure 8 that the characteristic frequency extracted from the power spectrum obtained by decomposing the signal through CKF is 104.7 Hz, and the theoretical characteristic frequency calculated from the bearing parameters of the test data is 104.5 Hz, and the error rate is 0.19%. Therefore, it can be accurately judged that this fault is an inner ring fault, which is consistent with the theory [19].

From the vibration signal analysed software of power spectrum, we can see that A1 power spectrum contains the fault feature frequency accompanied by frequency multi-

plication, which also contains some frequency; A2 power spectrum also contains the fault feature frequency with frequency multiplication However, the frequency is more than that of A1. The A3 power spectrum contains the characteristic frequency without frequency multiplication, but the frequency is more; the A4 power spectrum does not include the characteristic frequency [20]. Therefore, by comparison, the power spectrum of the instantaneous amplitude A1 of the PF1 component works best. This may be because the first PF component completely reflects the intrinsic nature of the signal, while the other PF components have separated by the first component.

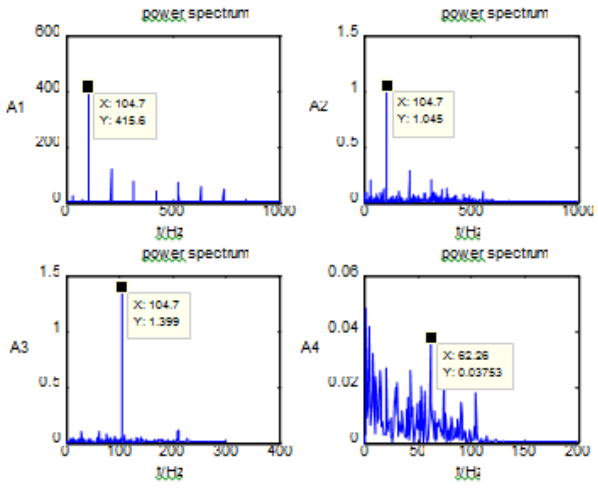

Figure 8: Outer ring faults A1, A2, A3, A4 power spectrum

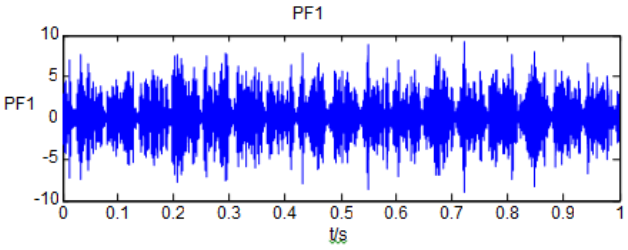

Figure 9: PF1 component diagram of rolling element failure

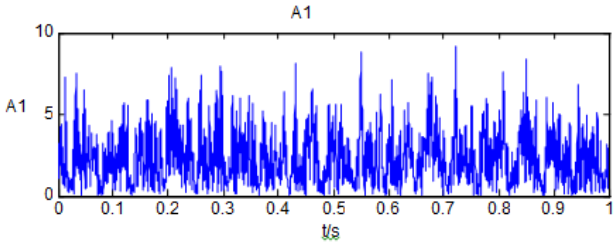

Figure 10: A1 component diagram of rolling element failure

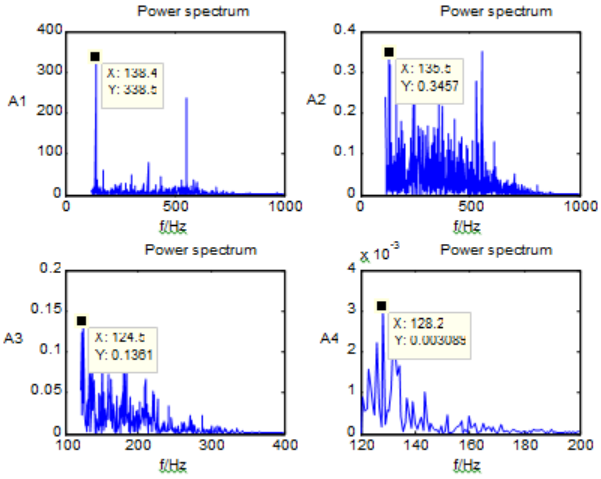

Figure 11: Enlarged power spectrum of rolling element faults A1, A2, A3 and A4

3.4.3 Analysis of rolling fault vibration signal

The designed vibration signal analysis software to analyse the test data to obtain Figure 9. The top of the software shows the time domain and frequency domain waveforms of the rolling element fault vibration signal. The bottom of the software shows the power spectrum of the first four instantaneous amplitudes of the PF component obtained after the vibration signal is decomposed by the CKF, from A1, A2, A3 power spectrum can be seen in the characteristic frequency of the inner ring fault is 138.4Hz. Figure 9, Figure 10, and Figure 11 show the PF1 component diagram, the A1 component diagram, and the A1-A4 power spectrum enlargement diagrams of the outer ring fault vibration signal, respectively.

From Figure 11, it can be seen that the characteristic frequency extracted from the power spectrum obtained by decomposing the signal through the CKF is 138.4 Hz, while the theoretical frequency calculated from the bearing parameters of the test data is 137.5 Hz, and the error rate is 0.66%. Therefore, it can be accurately determined that this fault is an inner ring fault, which is consistent with the theory [21]. From the vibration signal analysis software A power spectrum, we can see that A1 power spectrum contains the frequency of the fault feature at the same time, which also contains some of the frequency. A2 power spectrum also contains the fault feature frequency with frequency multiplication. However, it contains a large amount of noise; the A3 and A4 power spectra do not include the characteristic frequency, and there are many fre-

quency noises [7]. Therefore, by comparison, the power spectrum of the instantaneous amplitude A1 of the PF1 component works best. This may be because the first PF component completely reflects the intrinsic nature of the signal, while the other PF components are separated by the first component.

4 Conclusion

The CKF algorithm is used in a bearing fault diagnosis and estimation system composed of low precision, high-noise sensors, and the test data has repeatedly verified by the bearing spreader model. The test results show that the CKF algorithm can observe the sensor noise and the attitude disturbance noise. This article summarizes and draws on previous research results. Based on this, the local mean value decomposition has introduced into the fault diagnosis of rolling bearings. The fault characteristics of the vibration signal of rolling bearings are studied. In order to facilitate the analysis, the signal analysis software based on the CKF algorithm has designed by the MATLAB GUI tool for the actual bearing vibration signal. Through the study of this paper, we can draw the following conclusions as follows.

1. CKF is an adaptive time-frequency analysis method. This method can decompose complex multi-component AM/FM signals into the sum of several PF components with instantaneous physical meaning. It is very suitable for processing multi-component AM/FM signals through other methods. The comparison of time-frequency analysis methods reflects the superiority of this method.
2. Through the CKF decomposition of the vibration signal of the rolling bearing, the PF component has obtained, and then the power spectrum of the instantaneous amplitude is obtained, so that the fault characteristic frequency can be obtained for finding the fault point of the rolling bearing.
3. Combining the CKF algorithm with the MATLAB GUI, the fault diagnosis software for rolling bearings can be designed, the vibration signal is decomposed by CKF, and then its characteristic frequency is extracted to determine the fault point of the rolling bearing.

Acknowledgement: The authors declare that there is no conflict of interest regarding the publication of this paper. This work was supported by the National Natural Science Foundation of China (61403229,61503213,61403218), Natural Science Foundation of Zhejiang Province (LQ17F030005).

References

[1] Liu H., Wu W., Strong Tracking Spherical Simplex-Radial Cubature Kalman Filter for Maneuvering Target Tracking, J. Sensors., 2017,17(4), 741.
[2] Kowsari E., Safarinejadian B., Zarei J., Non-parametric fault detection methods in non-linear systems, J. IET Science, Measurement & Technology., 2016,10(3), 167-176.
[3] Zarei J., Shokri E., Robust sensor fault detection based on nonlinear unknown input observer. J. Measurement., 2014, 48, 355-367.
[4] Zhang A., Bao S., Bi W., Yuan Y., Low-cost adaptive square-root cubature Kalman filter for systems with process model uncertainty. J. Journal of Systems Engineering and Electronics.,2016, 27(5), 945-953.
[5] Brown T., Du S., Eruslu H., et al. Analysis of models for viscoelastic wave propagation,J. Applied Mathematics & Nonlinear Sciences., 2018, 3(1):55-96.
[6] Khellat F., Khormizi M., A global solution for a reaction-diffusion equation on bounded domains,J. Applied Mathematics & Nonlinear Sciences.,2018, 3(1): 15-22.
[7] Li X., Duan F., Mba D., Bennett I., Multidimensional prognostics for rotating machinery: A review,J. Advances in Mechanical Engineering.,2017, 9(2), 1687814016685004.
[8] Bian M., Wang J., Liu W., Qiu K., Robust and reliable estimation via recursive nonlinear dynamic data reconciliation based on cubature Kalman filter, J. Cluster Computing., 2017,20(4), 2919-2929.
[9] Al-Shabi M., Sigma-Point Filters in Robotic Applications, J. Intelligent Control and Automation.,2015, 6(03), 168.
[10] Shi Y., Che L., G, Q.,Zhou X., Adaptive high-degree Cubature Kalman filter with unknown noise statistics, J. JOURNAL OF INFORMATION & COMPUTATIONAL SCIENCE., 2014, 11(18), 6703-6712.
[11] Wang S., Zhang W., Yin C., Feng Y., Huber-based Unscented Kalman Filters with the q-gradient, J. IET Science, Measurement & Technology.,2017, 11(4), 380-387.
[12] Li H., An improved square root cubature particle filter for navigation, J. International Journal of Hybrid Information Technology.,2014, 7(6), 453-462.
[13] Wang L., Liang Y., Wang X., Xu L., Gaussian sum filter of Markov jump non-linear systems, J. IET Signal Processing.,2015, 9(4), 335-340.
[14] Foxlin E., Calloway T., Zhang H., Design and Error Analysis of a Vehicular AR System with Auto-Harmonization, J. IEEE transactions on visualization and computer graphics.,2015, 21(12), 1323-1335.
[15] Guo Y., Tharmarasa R., Rajan S., Song T. L., Kirubarajan T., Passive tracking in heavy clutter with sensor location uncertainty, J. IEEE Transactions on Aerospace and Electronic Systems.,2016, 52(4), 1536-1554.
[16] Li W., Wang Z., Yuan Y., Guo L., Particle filtering with applications in networked systems: a survey, J. Complex & Intelligent Systems.,2016, 2(4), 293-315.

[17] Havlík J.,Šimandl M.,Straka O., A New Practically Oriented Generation of Nonlinear Filtering Toolbox, J. Ifac Papersonline., 2015, 48(28): 1070-1075.

[18] Giron-Sierra J. M., Kalman Filter, Particle Filter and Other Bayesian Filters, Digital Signal Processing with Matlab Examples, 1rd ed. Volume 3. Springer Singapore, 2017.

[19] Roth M., Hendeby G., Gustafsson F., EKF/UKF maneuvering target tracking using coordinated turn models with polar/Cartesian velocity, International Conference on Information Fusion, IEEE, 2014:1-8.

[20] López-Salcedo J. A., Del Peral-Rosado J. A., Seco-Granados, G., Survey on robust carrier tracking techniques, J. IEEE Communications Surveys & Tutorials., 2014, 16(2), 670-688.

[21] Alhashimi A., Varagnolo D., Gustafsson T., Calibrating Distance Sensors for Terrestrial Applications Without Groundtruth Information, J. IEEE Sensors Journal., 2017, 17(12):3698-3709.